J Mater Sci (2008) 43:4737–4741
DOI 10.1007/s10853-007-2349-4

REACTIVITY OF SOLIDS

Morphology control of goethite acicular particles during aging by nitrogen bubbling and subsequent reactive aeration

Haruki Kurokawa · Mamoru Senna

Received: 27 July 2007 / Accepted: 27 November 2007 / Published online: 30 April 2008

Abstract Conditions for synthesizing acicular fine particles of goethite with high aspect ratio were devised by oxidizing mixed slurry comprising ferrous carbonate and hydroxide after neutralizing by alkali carbonate. By bubbling N_2 after neutralization into the slurry containing $FeCO_3$ and $Fe(OH)_2$, dissolved CO_2 is ejected. As a consequence, the relative concentration of CO_3^{2-} decreases and that of hydroxide increases. These favor the increase of the aspect ratio of the goethite particles via two factors, i.e., (1) decrease in the critical size of the nuclei and (2) suppression of growth inhibition at the tip of needle-like particles due to CO_3^{2-} adsorption. We propose a reaction scheme for the entire processing.

Introduction

Conventionally prepared goethite particles exhibit a needle-like shape due to its intrinsic crystallographical habit [1–5]. This is explained by the crystallographical contiguity between ferrous hydroxide and goethite with their common construction units, i.e., FeO_6 octahedra [6]. Since the phase conversion from goethite to maghemite, passing through hematite is entirely topotactic [7], the morphology of goethite is of particular importance for its final application to magnetic recording after the transformation to maghemite [2, 8].

Because of the crystallographical relationship between the hydroxide and oxyhydroxide, however, we often observe unfavorable dendritic twin structure in goethite [9]. When goethite contains twins in the form of dendrite, the magnetic properties of the final product, maghemite, become inferior [10]. Simultaneously, it is particularly desirable to prepare fine particulates with their axis length as small as possible, while maintaining high values of aspect ratio and surface area [11].

When we start from ferrous hydroxide or green rust (II) by alkali neutralization and subsequent oxidation in a conventional manner, the growth of the hydroxide cannot be adequately suppressed because of its high pH, leading to undesirable twin formation [12]. On top of that, these ferrous sources require low ferrous concentration and low temperature to decrease the productivity of goethite crystals [13].

From ferrous carbonate, in contrast, passing through the mixed state of carbonate–hydroxide mixture as a ferrous source, we may go up to higher concentrations and relatively high temperatures [14]. As we have recently reported on the differences in the ferrous source, starting from the carbonate–hydroxide mixture is really beneficial from various viewpoints, including morphology [13]. Twin formation can also be suppressed by starting from the mixture.

In the present study, we focus our effort on the suppression of the grain growth perpendicular to the principal axis of goethite to obtain smaller particles with higher aspect ratio, while avoiding twin formation. We found empirically that nitrogen bubbling before conventional oxidation processing by aeration results in goethite particles with higher aspect ratio. We, therefore, examine the role of nitrogen bubbling on morphology control by taking the sequential reaction processes into account.

H. Kurokawa
MS Company, Toda Kogyo Co., 1-4 Meiji Shinkai,
Otake 739-0652, Japan

M. Senna (✉)
Faculty of Science and Technology, Keio University,
3-14-1 Hiyoshi, Kohoku-ku, Yokohama 223-8522, Japan
e-mail: senna@applc.keio.ac.jp

Experimental

All of the experiments were carried out on a bench-scale plant, whose setup is schematically drawn in Fig. 1. The total capacity of the dispersed bubble reactor was 80 dm^3. The starting materials were aqueous solutions of ferrous sulfate (0.8 N) and sodium carbonate (1.6 N). These solutions were mixed and neutralized. The resulting slurry was aged at 47°C. Nitrogen bubbling was carried out at a constant flow rate of 50 dm^3/min. The slurry was further warmed to 53°C and aerated at constant flow rate, 90 dm^3/min, for the purpose of oxidation. The precipitate was filtered out, washed by de-ionized water until the specific conductance of the filtrate became less than 50 S/cm, and dried at 120°C for 3.5 h.

Changes in the pH and HCO_3^- concentration, as well as the total alkali concentration with aging time under the bubbling of either N_2 or air were monitored. The total alkali concentration was determined by conventional titration with 1 N HCl. The amount of CO_2 evolved was determined from the weight of $BaCO_3$ precipitated, after introduction to the aqueous solution of $Ba(OH)_2$, filtration, and drying.

We sampled the reaction mixture at appropriate time intervals and quenched the reaction by the quick addition of H_2O_2 aqueous solution to observe the morphology under a transmission electron microscope (JOEL, Model JEM-100S).

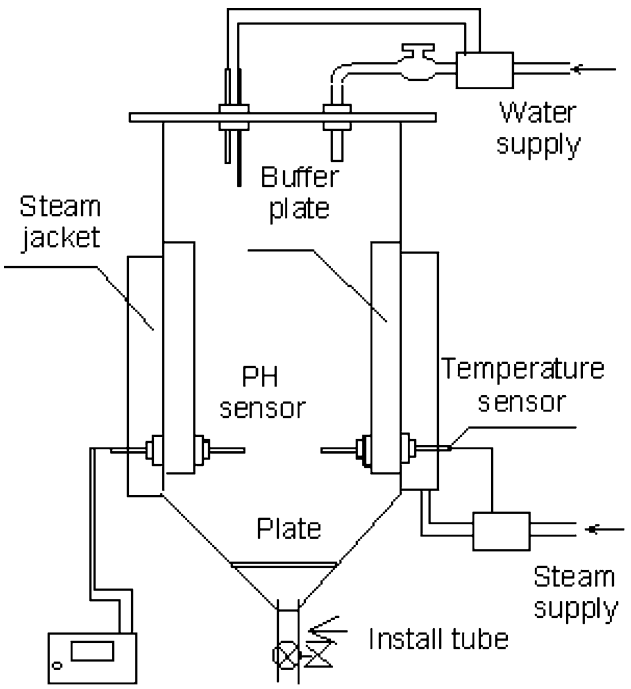

Fig. 1 Schematic diagram of the reactor with a bubble column

Results

Change in the chemical properties of slurries by N_2 bubbling and aero-oxidation

The change in pH of the slurry with aging time is plotted in Fig. 2. For the first 3.5 h, N_2 was bubbled. The flowing gas was then switched to air for oxidation. While a slight increase in pH from 9.3 to 9.5 is observed during N_2 bubbling, the pH decreases sharply when the flowing gas is changed from N_2 to air. This demonstrates the quick and efficient oxidation by aeration.

The change in the HCO_3^- concentration, as plotted in Fig. 3, is the opposite to that of the pH, i.e., slight decrease from 3.8 to 3.2 N during N_2 bubbling and sudden increase at the beginning of air oxidation. The total alkali concentration, in contrast, remained almost unchanged, with a very slight decrease, without any appreciable change at the moment of switching the gas from N_2 to air. As shown in Fig. 4, the evolution of CO_2 gas during N_2 bubbling is obvious. The rate of evolution tends to level off after 12 h to a steady state.

Morphology change by aging

Morphological change of the goethite particles obtained from the mixture of $FeCO_3$–$Fe(OH)_2$ is shown in Fig. 5,

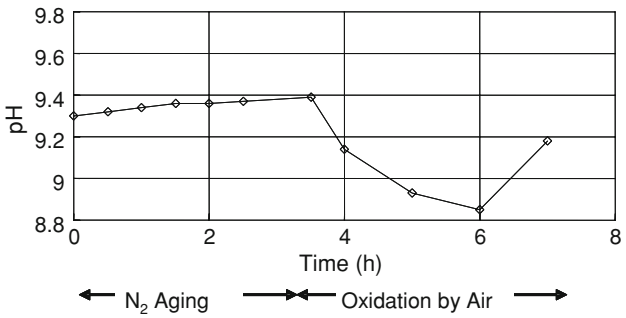

Fig. 2 Change in pH during N_2 aging and oxidation by air

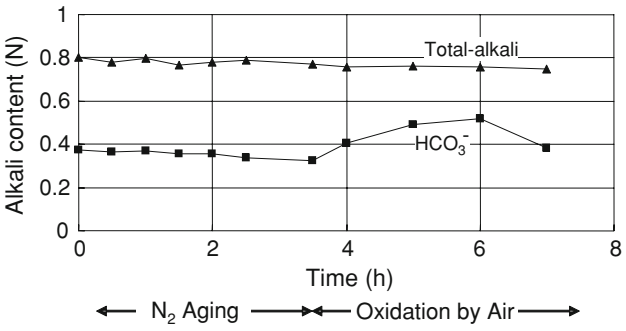

Fig. 3 Change in alkali content during N_2 aging and oxidation by air

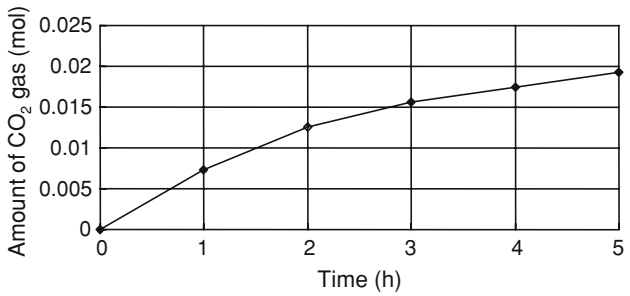

Fig. 4 Change in the amount of CO_2 evolved with N_2 bubbling time

with N_2 bubbling (Fig. 5a) and without bubbling (Fig. 5b). The aspect ratio increased by 20%, i.e., from 1:5 to 1:8 by N_2 bubbling for 5 h.

Change in the particle morphology with aging time is shown by starting from the mixture of $FeCO_3$−$Fe(OH)_2$ in Fig. 6, and from $Fe(OH)_2$ as a sole ferrous source in Fig. 7. Differences in the morphological development is clear by comparing Figs. 6 and 7. When we start from the mixture of $FeCO_3$−$Fe(OH)_2$ (Fig. 6), the goethite particles are thick from the beginning and preferentially grow in the direction of the *c*-axis. Nucleation of goethite from $Fe(OH)_2$ particles are, in contrast, thin and needle-like, and grow by maintaining a similar geometry (Fig. 7). Note that coexisting equiaxed particles, which also grow, are $Fe(OH)_2$. In both experiments, preliminary N_2 bubbling was carried out under the same conditions, i.e., flow rate of 50 dm^3/min.

Discussion

As we reported previously, starting from the mixture of $FeCO_3$−$Fe(OH)_2$ is beneficial as compared to starting from $Fe(OH)_2$ alone, due, amongst other reasons, to the higher throughput. It is, therefore, particularly noteworthy to increase the aspect ratio by N_2 bubbling [13]. We now try to elucidate

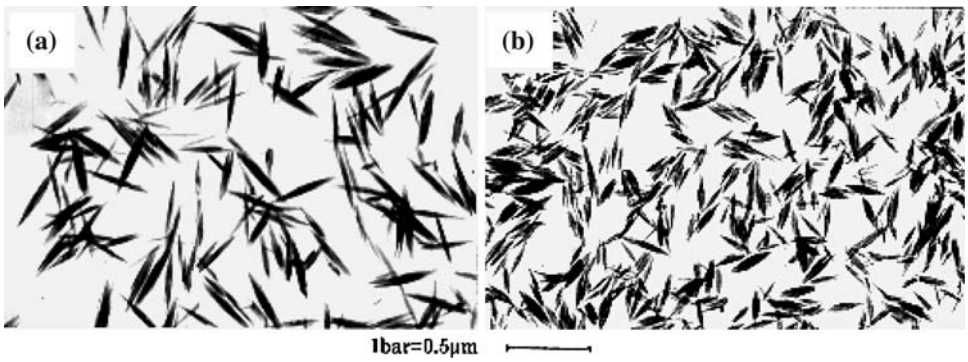

Fig. 5 Transmission electron micrographs of goethite particles: (**a**) with N_2 bubbling and (**b**) without N_2 bubbling

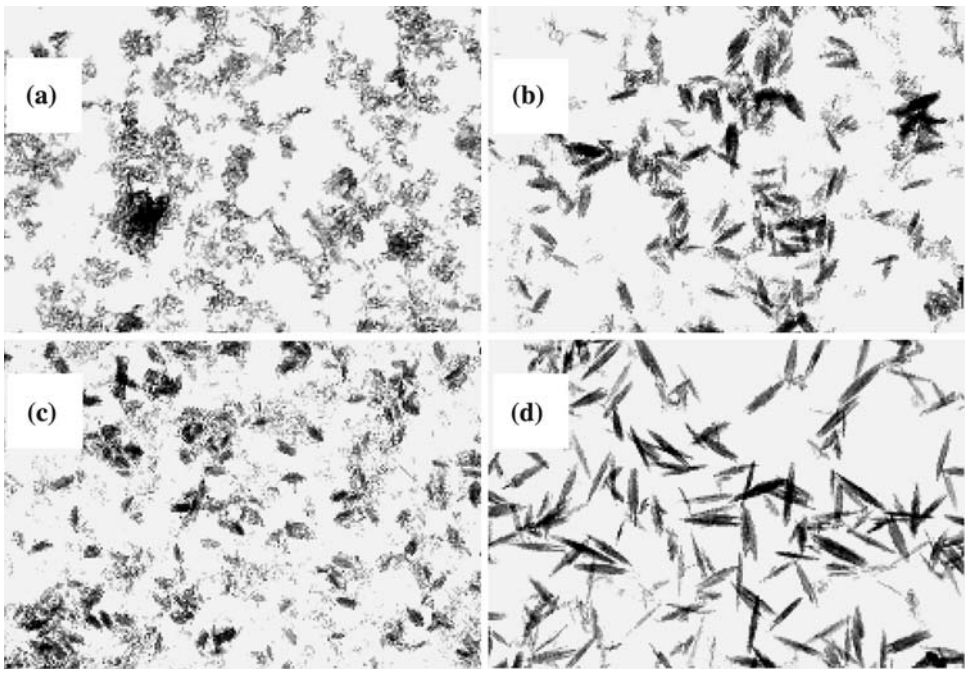

Fig. 6 Transmission electron micrographs of goethite particles from $FeCO_3$–$Fe(OH)_2$ with varying oxidation time: (**a**) just before oxidation, (**b**) after oxidation for 30 min, (**c**) 60 min, and (**d**) 150 min

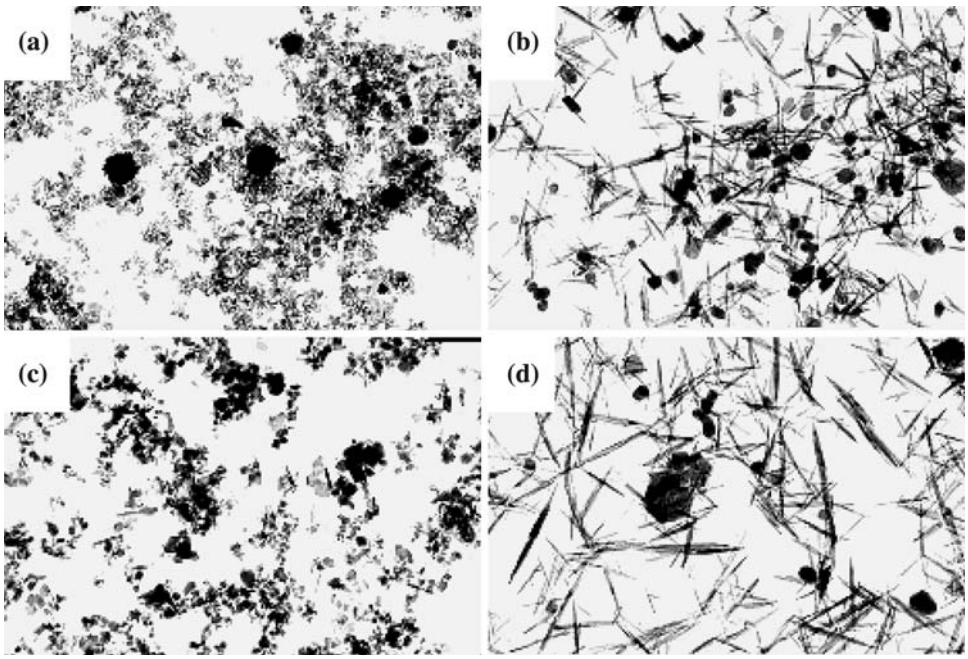

Fig. 7 Transmission electron micrographs of goethite particles from $Fe(OH)_2$ with varying oxidation time: (**a**) just before oxidation, (**b**) after oxidation for 30 min, (**c**) 120 min, and (**d**) 300 min

the chemical processes during N_2 bubbling and subsequent oxidation by aeration. As we observed previously, N_2 bubbling resulted in the effusion of CO_2, increase in pH, and decrease in the HCO_3^- concentration, without an eventual decrease in the alkali concentration. From these observations, we may propose the following reaction scheme:

1. Neutralization of excess ferrous sulfate by Na_2CO_3 and the formation of relatively stable ferrous carbonate and sodium sulfate, i.e., an exchange reaction:

$$FeSO_4 + Na_2CO_3 \rightarrow FeCO_3 + Na_2SO_4 \quad (1)$$

2. Hydrolysis of the remaining excess sodium carbonate:

$$Na_2CO_3 + H_2O \rightarrow NaHCO_3 + NaOH \quad (2)$$

3. Formation of the ferrous hydroxide:

$$FeCO_3 + 2NaOH \rightarrow Fe(OH)_2 + Na_2CO_3 \quad (3)$$

The overall reaction of iron carbonate with sodium carbonate, i.e., (1) + (2) + (3) from the above list, is:

$$FeCO_3 + Na_2CO_3 + 2H_2O \rightarrow Fe(OH)_2 + 2NaHCO_3 \quad (4)$$

When gaseous N_2 is introduced into the solution, dissolved CO_2 will be preferentially ejected, resulting in the hydrolysis of HCO_3^- as:

$$NaHCO_3 + H_2O \rightarrow NaOH + H_2O + CO_2 \uparrow \quad (5)$$

NaOH formed in the reaction of Eq. 5 again attacks acidic species, i.e., $FeCO_3$, to neutralize:

$$FeCO_3 + 2NaOH \rightarrow Fe(OH)_2 + Na_2CO_3 \quad (6)$$

When ferrous ions are titrated with NaOH in the low concentration range, where $Fe(OH)_2$ can be dissolved, the change is regarded as a simple acid–base reaction, as shown in Fig. 8, curve a. In contrast, the pH remains above 7, i.e., above the equivalent point, when the ferrous concentration is as high as 1.38 M, as shown in Fig. 8, curve b, since $Fe(OH)_2$ dissociates itself to release OH^-, i.e.:

$$Fe(OH)_2 \rightarrow Fe^{2+} + 2OH^- \quad (7)$$

Titration curves with Na_2CO_3 are shown in Fig. 9. When the ferrous concentration is low enough, white precipitates, $FeCO_3$, is formed, which is dissolved shortly after to give a clear green solution, as:

$$FeCO_3 + 2NaHCO_3 \rightarrow Fe(OH)_2 + Na_2CO_3 + 2CO_2 \uparrow \quad (8)$$

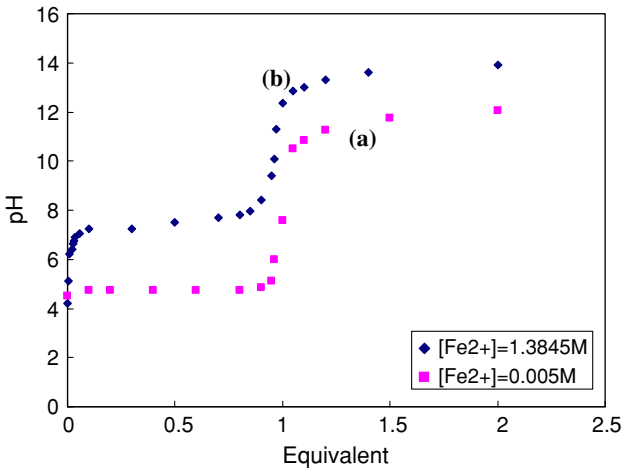

Fig. 8 Titration curves with NaOH with different ferrous concentrations: (**a**) 0.005 M and (**b**) 1.3845 M

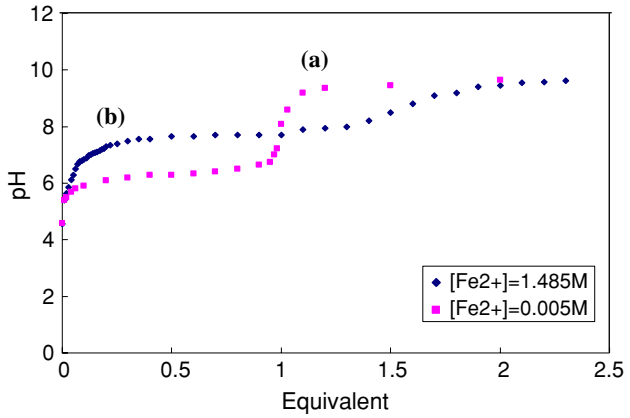

Fig. 9 Titration curves with Na_2CO_3 with different ferrous concentrations: (**a**) 0.005 M and (**b**) 1.3845 M

with pH value exceeding 7, as shown in Fig. 9, curve a. The increase in pH is explained by the change of acidic $FeCO_3$ to basic $Fe(OH)_2$. At higher ferrous concentrations, in contrast, white precipitate of $FeCO_3$ persisted. In the latter case, ferrous carbonate reacts partially with OH^-, like the reaction in Eq. 6, and, hence, the increase in pH remains sluggish, as shown in Fig. 9, curve b. According to Eq. 8, the consumption of HCO_3^- should be stoichiometrically corresponded to the formation of CO_2. Because of unavoidable incomplete capture efficiency of CO_2, this equivalence could not be experimentally verified.

To summarize the reaction scheme, dissolved CO_2 is ejected by bubbling N_2 after neutralization into the slurry containing $FeCO_3$ and $Fe(OH)_2$. As a consequence, the relative concentration of the hydroxide increases, decreasing the limit of the smallest goethite particles existing stably in the slurry, i.e., the critical radius of the goethite nuclei. This, in turn, increases the anisotropy of the goethite particles.

During aging, the relative concentration of $Fe(OH)_2$ increases by the reaction in Eq. 8, decreasing the size in the shorter axis direction, i.e., increase in the aspect ratio, as we observed in Fig. 5. We speculate that the coexistence of CO_3^{2-} ions in the vicinity of the nucleation site on the surface of $Fe(OH)_2$ increases the probability of inclusion of CO_3^{2-} ions in the nuclei by adsorption, increasing the critical radius of the nucleus. The adsorption of CO_3^{2-} ions simultaneously hinders the spontaneous growth process in the longer axis direction, making the particles chunkier. Although this speculation does not exhibit any contradiction with the observed results, we are presently seeking more direct evidence.

Conclusion

By bubbling N_2 after neutralization into the slurry containing $FeCO_3$ and $Fe(OH)_2$, dissolved CO_2 is ejected. As a consequence, the relative concentration of the hydroxide increases, decreasing the critical radius of the nuclei. This eventually increases the anisotropy of the goethite particles by suppressing growth in the direction of the shorter axis. The principal mechanism is based on the ejection of dissolved CO_2 by bubbling N_2 after neutralization into the slurry containing $FeCO_3$ and $Fe(OH)_2$. As a consequence, the relative concentration of CO_3^{2-} decreases and that of hydroxide increases. These favor the increase of the aspect ratio of the goethite via two factors, i.e., (1) decrease in the critical size of the nuclei and (2) suppression of growth inhibition at the tip of needle-like particles due to CO_3^{2-}.

References

1. Iwasaki M, Hara M, Ito S (2000) J Mater Sci 35:943. doi: 10.1023/A:1004710810785
2. Domingo C, Clemente RR, Blesa MA (1993) Solid State Ionics 59:187
3. Kosmulski M, Maczka E, Jartych E, Rosenholmb JB (2003) Adv Colloid Interface Sci 103:57
4. Sudakar C, Subbanna GN, Kutty TRN (2002) J Mater Chem 12:107
5. Sudakar C, Subbanna GN, Kutty TRN (2004) J Mater Sci 39:4271. doi:10.1023/B:JMSC.0000033409.26766.62
6. Subbanna GN, Sudakar C, Kutty TRN (2003) Mater Chem Phys 78:43
7. Cudennec Y, Lecerf A (2005) Solid State Sci 27:520
8. Varanda LC, Goya GF, Morales MP, Marques RFC, Godoi RHM, Jafelicci M, Serna CJ (2002) IEEE Trans Mag 38:1907
9. Löffler L, Mader W (2006) J Eur Ceram Soc 26:131
10. Debakker PMA, Degrave E, Van den Berghe RE, Bowen LH, Pollard RJ, Persoons RM (1991) Phys Chem Miner 18:131
11. SilesDotor MG, Bokhimi X, Morales A, Benaissa M, Cabral Prieto A (1997) Nanostructured Mater 8:657
12. Kurokawa H, Senna M (1999) Powder Technol 103:71
13. Kurokawa H, Senna M (2006) Mater Sci Eng B 135:55
14. Kurokawa H, Urai T (1996) J Jpn Soc Powder Powder Metall 43:52